ISSN (Print) 1226-1750
ISSN (Online) 2233-6656
Journal of Magnetics 24(2), 271-280 (2019) https://doi.org/10.4283/JMAG.2019.24.2.271

Analysis of Heat Transfer Enrichment in Hydromagnetic Flow of Hybrid Nanofluid Along Vertical Wavy Surface

M. Saleem Iqbal[1], Irfan Mustafa[2], and Abuzar Ghaffari[3]*

[1]*Department of Mathematics Islamabad College for Boys G-6/3, Islamabad 44000, Pakistan*
[2]*Department of Mathematics, Allama Iqbal Open University, H-8, Islamabad 44000, Pakistan*
[3]*Department of Mathematics, University of Education, Attock Campus 43600, Pakistan*

(Received 8 December 2018, Received in final form 3 June 2019, Accepted 4 June 2019)

The hybrid nanofluids are novel nanofluids and can be made by adding different types of nanoparticles in the plain fluid. The mathematical modeling of hybrid nanofluid under the magnetic influence over a vertical wavy surface is developed in the present theoretical investigation. The analysis is performed for hybrid nanofluid consisting of Al_2O_3-SiO_2 nanoparticles and compared with SiO_2 nanoparticle. The theoretical results also indicate that Al_2O_3-SiO_2 water hybrid nanofluid have higher heat transfer rate when compared with SiO_2- water nanofluid. In hybrid nanofluid, the choice of a suitable mixture of nanoparticles can lead to desire heat transfer phenomena. The implicit finite difference scheme is utilized for solution purposes. Results are presented in tabular and graphical form for the choice of suitable parameters.

Keywords : hybrid nanofluid, wavy surface, implicit finite difference, MHD

1. Introduction

With the advancement of technology, heat transfer enhancement is the utmost challenge for developing the Hi-technology industry. One way of improving the heat transfer is the addition to the plain liquid. Improvement of the heat transfer properties of the plain fluid can be achieved by increasing the thermal conductivity of the plain fluid. This can be attained by addition of metallic/ non-metallic nano-sized particles in the plain fluid termed as nanofluid [1, 2]. Because the nanofluid modifies the hydraulic and thermal properties of the plain fluid and causes heat transfer augmentation. Numerous researchers analyzed the thermophysical properties of the nanofluid [3-5].

In the recent past, the majority of the research is related to the nanofluid composed of single nanoparticle and their physical feathers are well established and discovered. Since the past decades, the vast majority of the researcher and scientist on nanofluid explored single type nanofluid. The qualities of this kind of nanofluid are very much characterized and investigated. The headway in nanomaterial has empowered the creation of hybrid nanoparticles (nanocomposites) and recently, there are some researchers investigated the characteristic of hybrid nanofluids. In this way, the motivation behind this article is to examine the characteristics of the newly developed hybrid nanofluids.

It appears that hybrid nanofluids have increased critical consideration among the thermal scientist. Hybrid nanofluid can be prepared through two techniques, firstly, suspending at least two sorts of nanoparticles into a plain liquid, secondly, suspending composites nanoparticles into plain liquid. The goal of inclusion of hybrid nanoparticles in the plain liquid is to enhance the convective transport properties of the plain fluid by means of mixing of nanomaterials' effective thermo-physical properties.

The fluids are assumed to be electrically conducting in many real-world applications and their ability to interact with the magnetic field applied ultimately leads to the study of magnetohydrodynamics. It is encountered in astrophysics and geophysics in various major processes. The main motivation in MHD flow and convective heat transfer is that fluid flow is regulated by the application of magnetic fields in naturally occurring phenomena. In various problems of mechanical engineering, namely MHD generators, plasma theory, and coolants. MHD natural convection flow has significant usage in the field

*Corresponding author: Tel: +923325505532
Fax: +923325505532, e-mail: abuzar.ghaffari@ue.edu.pk

of engineering, chemical, aeronautics heat exchangers, the cooling of reactors and electronics. In electromagnetic casting and ship propulsion, etc., such situations also occur most frequently. The field of magnetohydrodynamics is an active area of research based on these interesting applications.

Ma *et al.* [6] studied effects of the magnetic field and nanofluid on the natural convection heat transfer in a baffled U-shaped enclosure and shown that the heat transfer enhancement by introducing nanofluid decreases as increasing Rayleigh number. Izadi *et al.* [7] studied natural convective heat transfer of a magnetic nanofluid in a porous enclosure and found that the Nusselt number decreases first with increasing the strength ratio of the two magnetic sources. Sheikholeslami and Rashidi [8] investigated the effect magnetic field on free convection of Fe_3O_4-water nanofluid. Sheikholeslami *et al.* [9] analyzed three dimensional nanofluid flow and heat transfer in the presence of the magnetic field. They observed in both cases that increasing magnetic force results to decrease in the rate of heat transfer.

In recent studies, the authors [10-14] considered MWCNT-Fe_3O_4/water hybrid nanofluid to study heat transfer analysis using different cavity geometries and found that the average Nusselt number of each heater increases as the volume fraction of nanoparticles increases. The lattice Boltzmann method (LBM) has several advantages and can be applied for complex geometries and interfacial dynamics and Mohebbi *et al.* [15-19] and researchers [20-24] applied LBM for natural convection flow for nanofluid in different shapes of cavities and discussed the heat transfer at different locations and also Mohebbi *et al.* [25, 26] investigated forced convection for power-law fluid past a square cylinder between two parallel plates and in a channel with extended surface and concluded that in case of power-law fluid, heat transfer rate decreases with an increase in the power-law index and that the use of extended surfaces can enhance the rate of heat transfer for certain arrangements and multi-component fluid flows and heat conduction heat transfer enhancement using the lattice Boltzmann method. Also observed that the addition of nanoparticles to the pure fluid significantly enhanced the heat transfer. Ma *et al.* [27, 28] studied forced and natural convection heat transfer through a bent channel and square cylinder and found that the upstream control bar could reduce the aerodynamic drag effectively and heat transfer was more significant at high Reynolds number. Alsabery *et al.* [29] presented the impacts of local thermal non-equilibrium model and Al_2O_3-water nanofluid on natural convection heat transfer in a porous cavity and found that the heat transfer enhances by a sharper slope and especially at the higher value of the Darcy number. Ma *et al.* [30-32] explored natural convection heat transfer in hollow and U-shaped cavities in nanofluid and shown that the average Nusselt numbers in hot walls are higher than those in the cold wall. Also, the average Nusselt number of obstacle sides increased by increasing the Rayleigh number. Delouei *et al.* [33-34] examined effects of the ultrasonic vibration on the pressure drop and heat transfer enhancement of inlet turbulent flows and proved that effect of ultrasonic vibration on pressure drop and heat transfer enhancement diminishes with the growth of both Reynolds number and inlet temperature. Abchouyeh *et al.* [35] examined simulation of nanofluid natural convection in a channel with the presence of a sinusoidal obstacle and the highest value of heat transfer occurs at the highest Reynolds number. Ranjbar *et al.* [36] inspected that forced convection of nanofluid in a horizontal parallel-plate channel and found that the highest rate of heat transfer in the channel because of its highest degree of conductivity for copper water nanofluid. Izadi *et al.* [37-38] explored natural convection heat transfer of Cu-water nanofluid inside a porous and C-shaped cavities and proved that the average Nusselt numbers of both the fluid and solid phases increase as thermal conductivity ratio of the porous medium is enhanced and also average Nusselt number has a linear relation with the aspect ratio.

Balla et al. [39] investigated convective heat transfer by hybrid CuO-Cu nanofluid flow through the circular pipe and found that hybrid nanofluid shows good enhancement in the heat transfer as compared to simple nanofluid. Bhargava *et al.* [40] studied hybrid method on mixed convection flow of nanofluid on an inclined plane in a porous medium and shown that the concentration of nanoparticles decreases with increasing mixed convection parameter. Tayebi and Chamkha [41] analyzed natural convection in an annulus between two confocal elliptic cylinders filled with a Cu-Al_2O_3/water hybrid nanofluid and concluded that employing a Cu-Al_2O_3/water hybrid nanofluid is more efficient in heat transfer rate compared to the similar Al_2O_3/water nanofluid. S. Devi and A. Devi [42] discussed hybrid nanofluid flow over a three-dimensional stretching sheet and observed that heat transfer rate of Hybrid nanofluid (Cu-Al_2O_3/Water) is seemed to be higher than that of Nanofluid (Cu/Water). Takabi *et al.* [43] studied laminar forced convection of hybrid water-based suspension of Al_2O_3 and Cu nanoparticles in a heated circular tube and observed that hybrid suspension leads to a better thermal performance than the nanofluid.

The recent research work about the wavy surface and nanofluid are cited here. Shirvan *et al.* [44] investigated

influence of wavy surface characteristics on natural convection heat transfer in a cosine corrugated square cavity filled with Cu-water nanofluid and shown that the mean Nusselt number reduces by augmenting the wavy amplitudes while average Nusselt number increases Sheremet *et al.* [45] discussed natural convective heat transfer and fluid flow inside a porous wavy cavity filled with a nanofluid and noticed that local heat source has an efficient influence of the nanofluid flow and heat transfer rate. Cho [46] studied the natural convection heat transfer and entropy generation in a nanofluid-filled wavy-surface cavity subject to a horizontal magnetic field and shown that Nusselt number decreases with an increasing wave amplitude of the wavy surface. Siddiqa *et al.* [47] bi-convection flow with heat and mass transfer of a water-based nanofluid containing gyrotactic microorganisms over a vertical wavy surface and observed that the amplitude of the wavy surface has pronounced influence on the rates of heat and mass transfer. Sheremet *et al.* [48] investigated MHD natural convection in a wavy open porous tall cavity filled with a Cu-water nanofluid in the presence of an isothermal corner heater and concluded that Nusselt number is a decreasing function of the Hartmann number. Kameswaran *et al.* [49] discussed the convective heat transfer in the influence of nonlinear Boussinesq approximation, thermal stratification and convective boundary conditions on non-Darcy nanofluid flow over a vertical wavy surface and observed that increase in amplitude wavelength ratio tends to increase the average Nusselt number. Classical and preliminary work related to boundary layer flows along a wavy surface are given in [50-61].

In this paper, natural convection flow of hybrid nanofluid composed of two nanoparticles Al_2O_3 and SiO_2 through the vertical wavy surface is investigated. Heat transfer characteristics such as Nusselt number for two nanofluids are computed and compared with each other. For solving the system Keller-Box technique is employed.

2. Thermos Physical Properties of Nanofluid and Hybrid Nanofluid

The material properties of pure water and various nanoparticles are density, effective thermal conductivity, effective dynamic viscosity, heat capacity, and thermal expansion coefficient are given in Table 1. Hybrid Nanofluid is considered by taking the mixture of Al_2O_3 and SiO_2 nanoparticle into the water to form the required Hybrid nanofluid. The relations between the physical properties of nanofluid and hybrid nanofluid are listed in Table 2. Suffices 1, 2, *f, p, f, hnf* represent nanoparticles of Al_2O_3, nanoparticles of SiO_2, base fluid, nanoparticle, nanofluid and hybrid nanofluid respectively.

Table 1. Material properties of Al_2O_3, SiO_2 and base fluid.

Properties	C_p (J/KgK)	ρ (Kg/m^3)	κ (W/mK)	σ (S/m)	$\beta \times 10^{-5}$ (1/K)
Fluid (water)	4179	997.1	0.613	0.05	21.0
Al_2O_3	765	3970	40	3.5×10^7	0.85
SiO_2	703	2200	1.2	1×10^{-27}	0.056

Table 2. Thermo-physical properties of nanofluid and hybrid nanofluid.

Prosperities	Nanofluid	Hybird Nanofluid
Viscosity	$\mu_{nf} = \dfrac{\mu_f}{(1-\varphi)^{2.5}}$	$\mu_{hnf} = \dfrac{\mu_f}{(1-\varphi)^{2.5}}$
Thermal Conductivity	$\dfrac{\kappa_{nf}}{\kappa_f} = \dfrac{(\kappa_p + 2\kappa_f) - 2\phi(\kappa_f - \kappa_p)}{(\kappa_p + 2\kappa_f) + \phi(\kappa_f - \kappa_p)}$	$\dfrac{\kappa_{hnf}}{\kappa_f} = \dfrac{(\kappa_{hp} + 2\kappa_f) - 2\phi(\kappa_f - \kappa_{hp})}{(\kappa_{hp} + 2\kappa_f) + \phi(\kappa_f - \kappa_{hp})}$
Density	$\rho_{nf} = (1-\phi)\rho_f + \phi\rho_p$	$\rho_{hnf} = (1-\phi)\rho_f + \phi\rho_{hp}$
Heat capacity	$(\rho c_p)_{nf} = (1-\phi)(\rho c_p)_f + \phi(\rho c_p)_p$	$(\rho c_p)_{hnf} = (1-\phi)(\rho c_p)_f + \phi(\rho c_p)_{hp}$
Thermal Diffusivity	$(\rho\beta)_{nf} = (1-\phi)(\rho\beta)_f + \phi(\rho\beta)_p$	$(\rho\beta)_{hnf} = (1-\phi)(\rho\beta)_f + \phi(\rho\beta)_{hp}$
Electrical conductivity	$\dfrac{\sigma_{nf}}{\sigma_f} = 1 + \dfrac{3((\sigma_p/\sigma_f) - 1)\phi}{((\sigma_p/\sigma_f) + 2) - \phi((\sigma_p/\sigma_f) - 1)}$	$\dfrac{\sigma_{hnf}}{\sigma_f} = 1 + \dfrac{3((\sigma_{hp}/\sigma_f) - 1)\phi}{((\sigma_{hp}/\sigma_f) + 2) - \phi((\sigma_{hp}/\sigma_f) - 1)}$

where φ, ρ_{hp}, κ_{hp}, β_{hp}, C_{php} and σ_{hp} are
$\varphi = \varphi_1$ (Al_2O_3) + φ_2 (SiO_2), $\rho_{hp} = (\rho_1\varphi_1 + \rho_2\varphi_2)/\varphi$, $\kappa_{hp} = (\kappa_1\varphi_1 + \kappa_2\varphi_2)/\varphi$, $\beta_{hp} = (\beta_1\varphi_1 + \beta_2\varphi_2)/\varphi$, $C_{php} = (C_{p1}\varphi_1 + C_{p2}\varphi_2)/\varphi$, $\sigma_{hp} = (\sigma_1\varphi_1 + \sigma_2\varphi_2)/\varphi$.

3. Mathematical Modeling of the Problem

3.1. Geometrical configuration and assumptions

Fig. 1 show demonstration of the geometrical flow under consideration. It consists of the steady, laminar free convection flow and heat transfer of a nanofluid flowing through vertical wavy surface and shape of the wavy sheet is sinusoidal i.e. $\bar{y}_w = \bar{S}(\bar{x}) = \bar{\alpha} Sin\left(\frac{\pi \bar{x}}{l}\right)$, $\bar{\alpha}$ is the wave amplitude and l is the wavelength.

3.2. Boundary conditions

Under the above assumptions, the boundary conditions concerning the present study are described as [55-56, 59]

$$\begin{aligned} &\bar{y} = \bar{S}(\bar{x}): \bar{u} = 0,\ \bar{v} = 0,\ T = T_w, \text{ for all } \bar{x} > 0, \\ &\bar{y} \to \infty: \bar{u} = 0,\ \bar{p} = p_\infty,\ T = T_\infty \text{ for all } \bar{x} > 0. \end{aligned} \tag{1a}$$

where T is temperature, T_∞ is ambient temperature, T_w is wavy surface temperature, $\bar{p}$ is used to represent pressure, p_∞ is ambient pressure.

3.3. Governing equations of the flow problem

Coordinate system and flow scheme of the wavy plate is shown in Fig. 1. Using the assumptions stated in section 3.1, the two-dimensional mass, momentum and energy conservation laws have the form [55, 56, 59]

$$\nabla . V = 0, \tag{1b}$$

$$(V.\nabla).V = -(1/\rho_{nf})\nabla_p + \nabla^2 V + ((\rho\beta)_{nf}/\rho_{nf})g(T - T_\infty), \\ -(\sigma_{nf} B_0/\rho_{nf})V, \tag{2}$$

$$V = (\bar{u},\ \bar{v}) \tag{3}$$

$V = (\bar{u},\ \bar{v})$ represent velocity components along $(x,\ y)$ directions, T is used to represent temperature, σ_{nf} represents electric conductivity of nanofluid, $\bar{p}$ is used to represent pressure, ρ_{nf} be the density, B_0 be the strength of the uniform magnetic field applied perpendicular to the wavy plate. It is further assumed that magnetic Reynold number is so small that the induced magnetic field is neglected, T_∞ is used to represent ambient temperature and ∇^2 represents the Laplacian operator. A suitable set of dimensionless variables described as

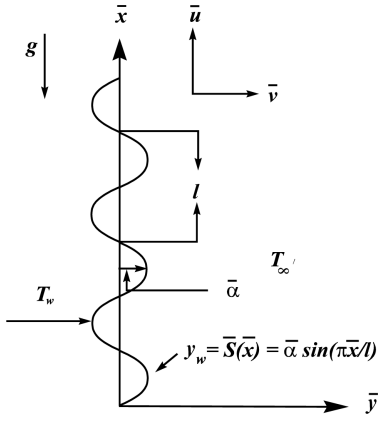

Fig. 1. Geometrical configurations of the current study.

$$\begin{aligned} &\xi = x = \frac{\bar{x}}{l},\ y = \frac{\bar{y} - \bar{S}(\bar{x})}{l} Gr^{\frac{1}{4}},\ u\frac{\rho_{fl}}{\mu_f} Gr^{-\frac{1}{2}}\bar{u}, \\ &v = \frac{\rho_{fl}}{\mu_f} Gr^{-\frac{1}{4}}(\bar{v} - S_\xi \bar{u}), \\ &S = \frac{\bar{S}(\bar{x})}{l},\ \theta(\xi,\ \eta) = \frac{T - T_\infty}{T_w - T_\infty},\ \psi(\xi,\ \eta) = \xi^{\frac{3}{4}} f(\xi,\ \eta), \\ &\eta = \xi^{-\frac{1}{4}} y,\ \Omega = \sqrt{1 + S_\xi^2},\ M = \frac{Q l^2}{\mu_f Gr^{\frac{1}{2}} (\rho c_p)_f},\ p = \frac{l^2}{\nu^2 \rho_f} Gr^{-\frac{1}{4}} \bar{p}, \\ &Gr = \frac{g\beta_f (T_w - T_\infty) l^3}{\nu_f^2},\ u = \frac{\partial \psi}{\partial x},\ v = \frac{\partial \psi}{\partial y}, \end{aligned} \tag{4}$$

using the above set of transformations, a non-dimensional system of equations under the boundary layer assumptions takes the form as

$$\frac{\Omega^2}{A_1} f''' + \frac{3}{4} f f'' - \xi\left(\frac{1}{2} + \frac{\Omega_\xi}{\Omega}\xi\right)(f')^2 - \xi^{1/2}\left(\frac{MA_4}{A_2\Omega_2}\right) f' \\ - \frac{A_4}{A_2\Omega^2}\theta = \xi\left[f'\frac{\partial f'}{\partial \xi} - f''\frac{\partial f}{\partial \xi}\right], \tag{5}$$

$$\frac{A\Omega^2}{A_3 Pr}\theta'' + \frac{3}{4} f\theta = \xi\left[f'\frac{\partial \theta}{\partial \xi} - \theta'\frac{\partial f}{\partial \xi}\right], \tag{6}$$

where Pr and M represent the Prandtl and magnetic numbers respectively. The subscript ξ denotes derivative with respect to ξ and the $'$ represents the differentiation w.r.t η. The parameter Ω is the wavy effect in the leading equations. Whereas A_1, A_2, A_3, A_4 and A are the nanofluid constants parameters given in Table 3. Equation (4) in non-dimensional form can be expressed as

$$\begin{aligned} &f(\xi,\ 0) = 0,\ f'(\xi,\ 0) = 0,\ \theta(\xi,\ 0) = 1, \\ &f'(\xi,\ \infty) = 0,\ \theta(\xi,\ \infty) = 0. \end{aligned} \tag{7}$$

Entreating equation. (4) local Nusselt number Nu and local skin friction coefficient C_f in the non-dimensional form are given by

$$\begin{aligned} &C_f = C_{fx}(Gr/x)^{1/4} = \frac{\Omega}{(1 - \phi)^{2.5}} f''(\xi,\ 0), \\ &Nu = Nu_x (Grx^3)^{-1/4} = \Omega \frac{\kappa_{nf}}{\kappa_f}\theta'(\xi,\ 0) \end{aligned} \tag{8}$$

Table 3. Nanofluid constant parameters.

$$A_1 = (1-\phi)^{2.5}[1-\phi+\phi(\rho_p/\rho_f)],\ A_2 = [1-\phi+\phi(\rho_p/\rho_f)],\ A = \frac{\kappa_{nf}}{\kappa_f},$$

$$A_3 = \left[1-\phi+\phi\left(\frac{(\rho c_p)_p}{(\rho c_p)_f}\right)\right],\ A_4 = 1+\left(\frac{3((\rho_p/\rho_f)-1)\phi}{((\rho_p/\rho_f)+2)-\phi((\rho_p/\rho_f)-1)}\right).$$

4. Numerical Solution

The equations (5)-(7) related to the present study are simulated through a finite difference scheme [62, 63]. The computed results are accurate up to 10^{-6}. A uniform step size of 0.005 and 3000 and 400 grid points was used in η and ξ-direction. We took infinity as 20 which is sufficiently large for an accurate solution. In order to assure the reliability and accuracy and of numerical results, uniform grids test has been executed for the current problem. The grid independence of the current numerical solution was tested by constructing a number of tries for different step sizes for variables η and ξ. It is noticed that there is no variation in the numerical solution when $\Delta\eta < 0.005$ and $\Delta\xi < 0.005$. A grid independent test for the current method is included in Table 4. In order to solve by Keller-Box method, the following procedure is followed. Given equations are reduced into the system of first-order equations. To get the finite difference equation with second-order truncation error simple center difference formula for derivative and average of the midpoint and net rectangle is used. The resulting finite difference equations were nonlinear algebraic equations which had linearized by using Newton's method. The block factorization scheme is applied to calculate the inverse of the coefficient matrix of the finite difference equations. For the confirmation of the predicted results, the comparison was made with the values of $C_{fx}Re_x^{1/2}$, $Nu_xRe_x^{-1/2}$ $f''(0,0)$ and $-\theta'(0,0)$ as given in Tables 5 and 6. These Tables illustrates that the numerical values of these physical quantities support very closely with the earlier available data.

Table 4. Gird independence test when $\phi = 0.0$, Pr = 0.62, α = 0.1, M = 0.2.

No of grid points η direction With fix $\eta = 20$.	No of grid points ξ direction With fix $\xi = 1$.	$-C_f$	Nu
100	10	0.85303	0.31679
200	20	0.85304	0.31685
400	50	0.85313	0.31687
800	100	0.85313	0.31687
1600	200	0.85313	0.31687
3200	400	0.85313	0.31687

Table 5. Computed values of $C_{fx}(Gr/x)^{1/4}$ and $Nu_x(Grx^3)^{-1/4}$, when $\alpha = 0$, $\xi = 2$.

Pr	$C_{fx}(Gr/x)^{1/4}$		$Nu_x(Grx^3)^{-1/4}$	
	Present	Alim *et al.* [64]	Present	Alim *et al.* [64]
0.72	0.74643	0.74641	0.33683	0.33715
1.5	0.66054	0.6690	0.43354	0.43391
3.0	0.58201	0.58220	0.54120	0.54159
4.5	0.53822	0.53827	0.61241	0.61277
7.0	0.49270	0.49260	0.69782	0.69810

5. Results and Discussion

A system of non-linear partial differential equations, which represents the dimensionless form of a mathematical model based on natural convection flow of hybrid nanofluid along the vertical wavy surface is solved numerically by applying implicit finite scheme [62- 63]. Hybrid nanofluid is a mixture of Al_2O_3-water and SiO_2-water nanofluids. The influence of pertinent parameters namely, magnetic (M), athe mplitude of the waviness (α)

Table 6. Comparison of values $f''(0,0)$ and $-\theta'(0,0)$ when $\alpha = \xi = 0$.

Pr	$f''(0,0)$			$-\theta'(0,0)$		
	Present	Hossain [65]	Alim *et al.* [64]	Present	Hossain [65]	Alim *et al.* [64]
1	0.9082	0.908	0.90814	0.4010	0.401	0.40101
10	0.5928	0.591	0.59269	0.8268	0.825	0.82663
25	0.4876	0.485	0.48733	1.0690	1.066	1.06847
50	0.4176	0.485	0.41727	1.2896	1.066	1.28879
100	0.3559	0.352	0.35559	1.5495	1.542	1.54827

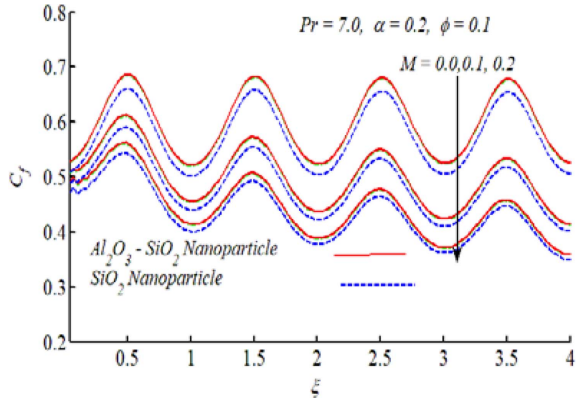

Fig. 2. (Color online) Magnetic effect on Skin friction.

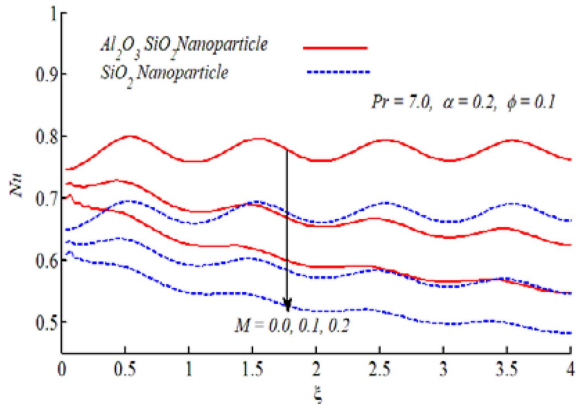

Fig. 3. (Color online) Magnetic effect on Nusselt Number.

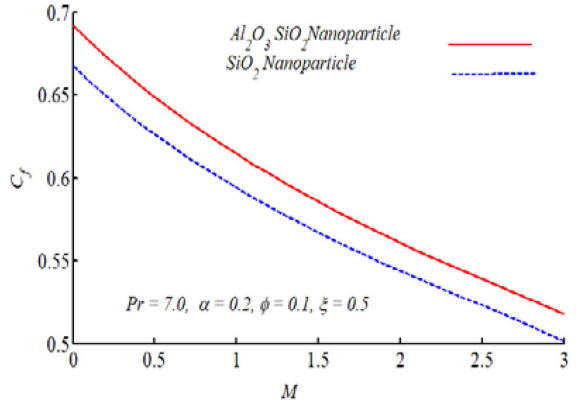

Fig. 4. (Color online) Skin friction against *M*.

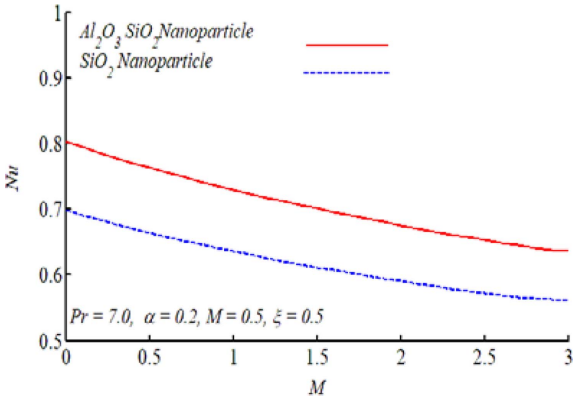

Fig. 5. (Color online) Nusselt number versus *M*.

and nanoparticles concentration (ϕ) on physical quantities, like skin friction coefficient (C_f) and Nusselt number (Nu) are discussed graphically. The solid line represents the behavior of hybrid nanofluid and dashed line represents SiO_2-water nanofluid. In this study, the concentration of nanoparticles in a base fluid like water is considered up to 10 %. Figures 2 and 3 depict the effects of the magnetic parameter on the skin friction coefficient (C_f) and Nusselt number (Nu), while the other parameters are kept fixed and labeled in Figs. for better understanding of the readers.

From Fig. 2 it is concluded that magnetic field produces Lorentz force which acts as a retarding force, therefore, the skin friction coefficient decreases for both hybrid and SiO_2-water nanofluids. The values of skin friction coefficient in case of hybrid nanofluid become higher as compared to SiO_2-water nanofluid. Figure 3 shows that Nusselt number also decreases with the increase of magnetic parameter, this is due to the fact that temperature within nanofluid become higher and consequently, heat transfer rate reduces at the surface. The values of Nusselt number still higher for hybrid nanofluid as compared to SiO_2-water nanofluid. It is also concluded that both skin friction coefficient (C_f) and Nusselt number (Nu) become a decreasing function along the wavy surface. For the validation of magnetic effects as observed in Figs. 2 and 3, the graphical results of skin friction coefficient and Nusselt number against M (magnetic number) are plotted in Figs. 4 and 5. It is elucidated from Figs. 4 and 5, both the skin friction and Nusselt number decrease with the increase of M. In the case of hybrid nanofluid, the values of both skin friction and Nusselt number become maximum

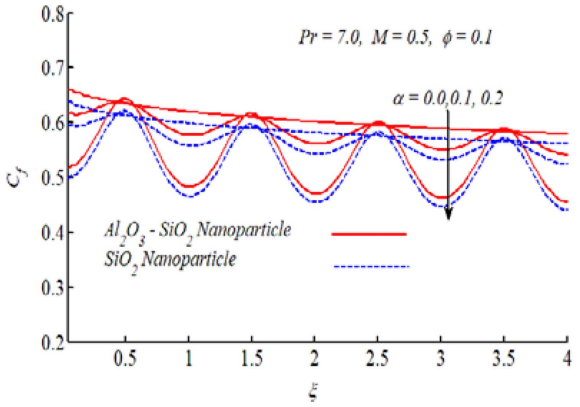

Fig. 6. (Color online) Effect of waviness on skin friction.

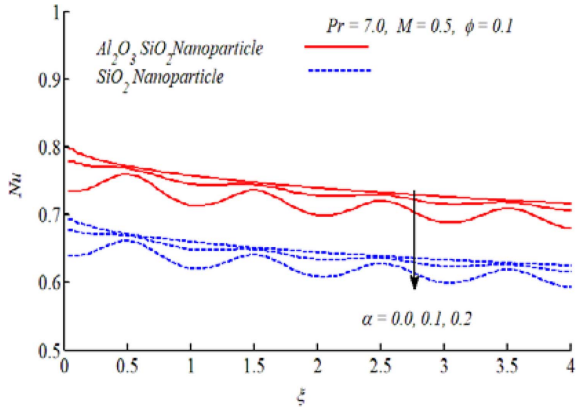

Fig. 7. (Color online) Effect of waviness on Nusselt Number.

than the SiO_2-water nanofluid, whereas, this decrease reduces with the increase of magnetic strength.

Figures 6 and 7 illustrate the variation of local skin friction and local Nusselt number against different amplitude to wavelength ratio α. Overall, local skin friction decreases with the increase of α but it higher in the case of hybrid nanofluid in comparison to SiO_2 nanofluid as seen from Figure 6. Figure 7 illustrates that Local Nusselt

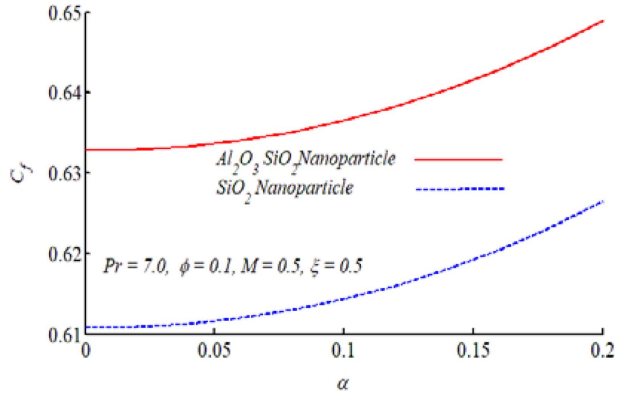

Fig. 8. (Color online) Skin friction graph versus α.

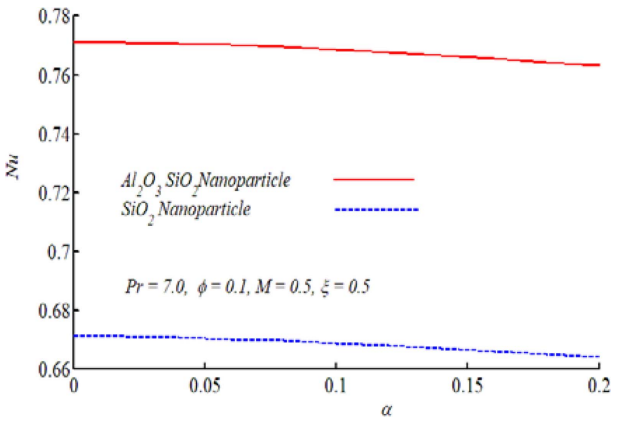

Fig. 9. (Color online) Nusselt number against α.

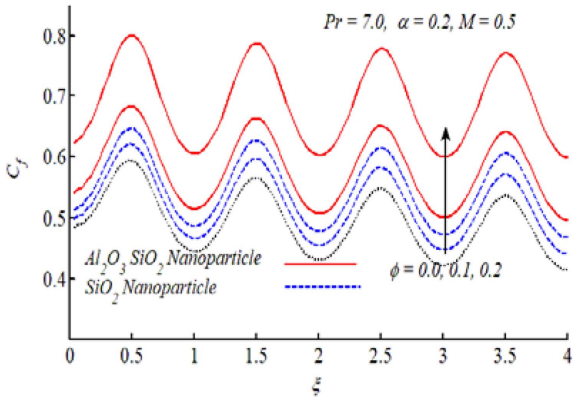

Fig. 10. (Color online) Graph of skin friction influenced by ϕ.

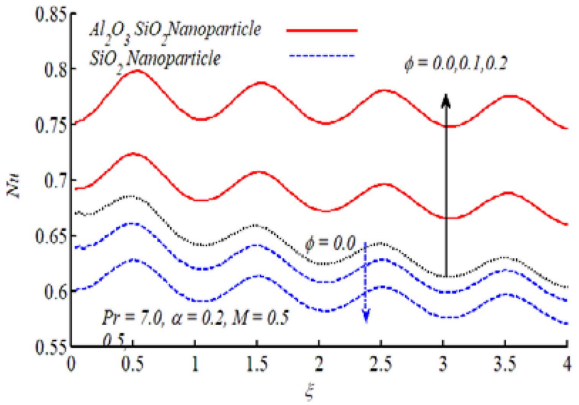

Fig. 11. (Color online) Graph of Nusselt number influenced by ϕ.

number also decreases with the increase of α, but for hybrid nanofluid, it is higher than the SiO_2 nanofluid. Local friction factor and local heat transfer rate verses α plotted in Figures 8 and 9. Local skin friction is maximum for hybrid nanofluid in comparison to the SiO_2-water nanofluid, on the other hand, the local heat transfer rate for hybrid nanofluid is higher in comparison to SiO_2 nanofluid is portrayed through these figures. Skin

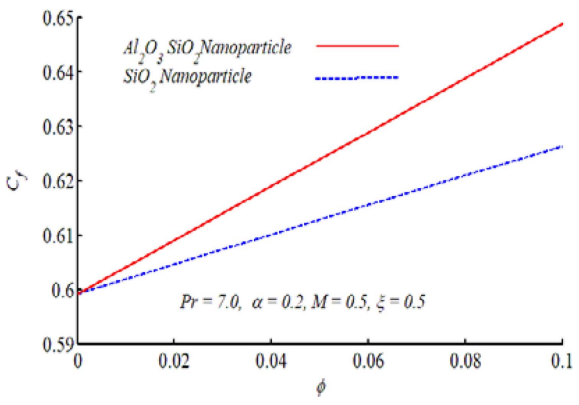

Fig. 12. (Color online) Skin friction variation against ϕ.

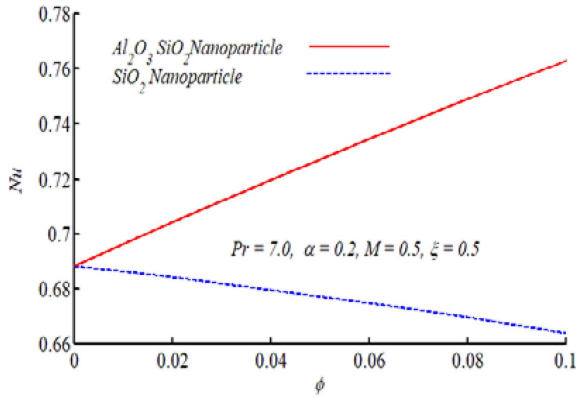

Fig. 13. (Color online) Nusselt number variation for different ϕ.

friction higher for hybrid nanofluid as compared to SiO_2-water nanofluid observed from Figure 6 and the Nusselt number is greater than the SiO_2 nanofluid. Therefore, by adjusting the appropriate concentration of Al_2O_3 nanoparticles the heat transfer phenomena can be increased or decreased as depicted in Figure 7.

Skin friction and Nusselt number against solid volume fraction are plotted in Figures 10 and 11. From these figures, it is seen that both skin friction and Nusselt number for hybrid nanofluid is higher as compared to the SiO_2 nanofluid. The graphical results of skin friction coefficient and Nusselt number against ϕ (concentration of nanoparticles) are plotted in Figs. 12 and 13. It is revealed from Figs. 12 and 13, both the skin friction and Nusselt number increase with the increase of ϕ. In the case of hybrid nanofluid, the values of both skin friction and Nusselt number become maximum than the SiO_2-water nanofluid, whereas, Nusselt number decreases with the increase of concentration of SiO_2 nanoparticle.

Table 7. Values of skin friction and Nusselt number for variation φ_1 and φ_2 Al_2O_3-SiO_2 hybrid nanofluid when $M = 0.5$, Pr = 6.2, $\alpha = 0.2$.

ξ	φ_1	φ_2	C_f	Nu
0.5	0.0	0.0	0.5942	0.6856
	0.0	0.1	0.6203	0.6608
	0.05	0.05	0.6430	0.7599
	0.1	0.0	0.6449	0.7698
1.0	0.0	0.0	0.4451	0.6432
	0.0	0.1	0.4667	0.6227
	0.05	0.05	0.4828	0.7140
	0.1	0.0	0.4846	0.7241
1.5	0.0	0.0	0.5652	0.6591
	0.0	0.1	0.5955	0.6396
	0.05	0.05	0.6178	0.7365
	0.1	0.0	0.6193	0.7457
2.0	0.0	0.0	0.4312	0.6260
	0.0	0.1	0.4560	0.6106
	0.05	0.05	0.4706	0.6987
	0.1	0.0	0.4726	0.7089

Table 8. Values of skin friction and Nusselt number for variation of φ_1 for Al_2O_3-SiO_2 hybrid nanofluid when $\varphi_2 = 0.05$, $M = 0.5$, Pr = 6.2, $\alpha = 0.2$.

ξ	φ_1	C_f	Nu
0.5	0.0	0.6073	0.6743
	0.01	0.6213	0.7195
	0.02	0.6273	0.7324
	0.03	0.6327	0.7424
	0.04	0.6379	0.7513
	0.05	0.6430	0.7599
1.0	0.0	0.4560	0.6340
	0.01	0.4660	0.6755
	0.02	0.4706	0.6877
	0.03	0.4748	0.6972
	0.04	0.4788	0.7058
	0.05	0.4828	0.7140
1.5	0.0	0.5084	0.6505
	0.01	0.5947	0.6953
	0.02	0.6010	0.7083
	0.03	0.6067	0.7184
	0.04	0.6123	0.7277
	0.05	0.6178	0.7365
2.0	0.0	0.4436	0.6194
	0.01	0.4530	0.6595
	0.02	0.4578	0.6718
	0.03	0.4621	0.6815
	0.04	0.4664	0.6903
	0.05	0.4706	0.6987
	0.2	0.4944	0.8897

Tables 6 and 7 are constructed for numerical data for C_f and Nu for the variation of concentration of Al_2O_3 (φ_1) and SiO_2 (φ_2) in Al_2O_3-SiO_2 hybrid nanoparticle at three different locations, $\xi = 0.5$, $\xi = 1.0$, $\xi = 1.5$ and $\xi = 2.0$ along the wavy surface. From Tables 5 and 6, it is noticed that with the increase of concentration of Al_2O_3 nanoparticle heat transfer rate increases whereas with the increase of concentration of SiO_2 nanoparticle heat transfer decreases. Therefore, by adjusting the proportion of these nanoparticles in Al_2O_3-SiO_2 hybrid nanoparticle heat transfer rate can be achieved according to the requirement.

6. Concluding Remarks

The present analysis is to study the heat transfer rate due to Al_2O_3-SiO_2 hybrid nanofluid through a vertical

wavy surface in the presence of MHD. This problem is converted in mathematical form and solved numerically by a famous Keller-box scheme. The tabular and graphical mod is used to elaborate on the obtained results. This study concludes that

1. Heat transfer rate is higher on the wavy surface as compared to a flat surface.
2. The copper nanoparticle has a good impact on the heat transfer rate as compared to the silver nanoparticle.
3. Heat transfer rate is remarkably increased with the increase of nanoparticle volume fraction.
4. Magnetic field opposes the heat transfer rate and retards the fluid flow at the surface.
5. The skin friction coefficient and rate of heat transfer decrease for increasing values of the amplitude of the wavy surface and magnetic parameter *M*.

References

[1] S. U. S. Choi, ASME Publications FED **231**, 99 (1995).
[2] S. U. S. Choi, Z. G. Zhang, W. Yu, F. E. Lockwood, and E. A. Grulke, App. Phy. Lett. **79**, 2252 (2001).
[3] Y. Ding, H. Chen, L. Wang, C. Y. Yang, Y. He, W. Yang, W. P. Lee, L. Zhang, and R. Huo, KONA **25**, 23 (2007).
[4] S. K. Das, S. U. S. Choi, and H. E. Patel, Heat Transf. Eng. **27**, 3 (2006).
[5] M. S. Liu, C. C. Lin, I. T. Huang, and C. C. Wang, Int. Comm. Heat Mass Transf. **32**, 1202 (2005).
[6] Y. Ma, R. Mohebbi, M. M. Rashidi, Z. Yang, and M. A. Sheremet, Int. J. Heat Mass Transfer **130**, 123 (2019).
[7] M. Izadi, R. Mohebbi, A. A. Delouei, and H. Sajjadi, Int. J. Mech. Sci. **151**, 154 (2019).
[8] M. Sheikholeslami and M. M. Rashidi, Journal of the Taiwan Institute of Chemical Engineers **56**, 6 (2015).
[9] M. Sheikholeslami, M. G. Bandpy, and H. R. Ashorynejad, Physica A: Statistical Mechanics and its Applications **432**, 58 (2015).
[10] M. Izadi, R. Mohebbi, D. Karimi, and M. A. Sheremet, Chem. Eng. Process. **125**, 56 (2018).
[11] R. Mohebbi and M. M. Rashidi, J. Taiwan Inst. Chem. Engrs. **72**, 70 (2017).
[12] Y. Ma, R. Mohebbi, M. M. Rashidi, and Z. Yang, J. Therm. Anal. Calorim. **136**, 1723 (2019).
[13] H. Sajjadi, A. A. Delouei, M. Izadi, and R. Mohebbi, Int. J. Heat Mass Transfer. **132**, 1087 (2019).
[14] A. Matori, R. Mohebbi, Z. Hashemi, and Y. Ma, J. Therm. Anal. Calorim. 1 (2019).
[15] R. Mohebbi and M. M. Rashidi, J. Taiwan Inst. Chem. Eng. **72**, 70 (2017).
[16] R. Mohebbi, M. Izadi, and A. J. Chamkha, Phys. Fluids **29**, 122009 (2017).
[17] R. Mohebbi, K. S. Haghighi, and Y. Ma, J. Appl. Fluid Mech. **12**, 1151 (2019).
[18] R. Mohebbi, M. Izadi, M., N. A. C. Sidik, and G. Najafi, Int. J. Number. Method H (2018).
[19] R. Mohebbi, S. M. A. Mehryan, M. Izadi, and O. Mahian, J. Therm. Anal. Calorim. 1 (2019).
[20] M. Nazari, M. H. Kayhani, and R. Mohebbi, Int. J. Mod. Phys. C **24**, 1350060 (2013).
[21] M. Nazari, R. Mohebbi, and M. H. Kayhani, J. Non-Newton Fluid **204**, 38 (2014).
[22] R. Mohebbi, M. Nazari, and M. H. Kayhani, J. Appl. Mech. Tech. Ph. **57**, 55 (2016).
[23] H. Heidari, R. Mohebbi, and A. Safarzade, J. Ponte Int. Sci. Res. J. **72**, (2016).
[24] R. Mohebbi and H. Heidari, Int. J. Mod. Phys. C **28**, 1750042 (2017).
[25] R. Mohebbi, H. Lakzayi, N. A. C. Sidik, and W. M. A. A Japan, Int. J. Heat Mass Transfer **117**, 425 (2018).
[26] R. Mohebbi, M. M. Rashidi, M. Izadi, N. A. C. Sidik, and H. W. Xian, Int. J. Heat Mass Transfer **117**, 1291 (2018).
[27] Y. Ma, R. Mohebbi, M. M. Rashidi, and Z. Yang, Physics of Fluids **30**, 032001 (2018).
[28] Y. Ma, R. Mohebbi, M. M. Rashidi, and Z. Yang, Int. J Mod. Phys. C **29**, (2018).
[29] A. I. Alsabery, R. Mohebbi, A. J. Chamkha, and I. Hashim, Chem. Eng. Sci. https://doi.org/10.1016/j.ces.2019.03.006 (2019).
[30] Y. Ma, R. Mohebbi, M. M. Rashidi, and Z. Yang, Int. J. Number. Method H **29**, 223 (2019).
[31] Y. Ma, R. Mohebbi, M. M. Rashidi, and Z. Yang, J. Taiwan Inst. Chem. Engrs. **93**, 263 (2018).
[32] Y. Ma, R. Mohebbi, M. M. Rashidi, and Z. Yang, J. Therm. Anal. Calorim. 1 (2019).
[33] A. A. Delouei, H. Sajjadi, M. Izadi, and R. Mohebbi, Appl. Therm. Eng. **146**, 268 (2019).
[34] A. A. Delouei, H. Sajjadi, R. Mohebbi, and M. Izadi, Ultrason. Sonochem. **51**, 151 (2019).
[35] M. A. Abchouyeh, R. Mohebbi, and O. S. Fard, Int. J. Mod. Phys. C **29**, 1850079 (2018).
[36] P. Ranjbar, R. Mohebbi, and H. Heidari, Int. J. Mod. Phys. C **29**, 1 (2018).
[37] M. Izadi, G. Hoghoughi, R. Mohebbi, and M. A. Sheremet, J. Mol. Liq. **261**, 357 (2018).
[38] M. Izadi, R. Mohebbi, A. J. Chamkha, and I. Pop, Int. J. Number. Method H **28**, 1930 (2018).
[39] H. H. Balla, S. Abdullah, W. M. Faizal, R. Zulkifli, and K. Sopian, J. Oleo Sci. **62**, 533 (2013).
[40] R. Bhargava, Pratibha, and H. Chandra, Int. J. App. Comp. Math. 1-20, DOI 10.1007/s40819-016-0278-0.
[41] T. Tayebi and A. J. Chamkha, Num. Heat Transf., Part A: Appli. **7**, 1141 (2016).
[42] S. S. U. Devi and S. A. Devi, Can. J. Phy. **94**, 4900 (2016).
[43] B. Takabi, A. M. Gheitaghy, and P. Tazraei, J. Therm. Heat Transf. 523 (2016).
[44] K. M. Shirvan, R. Ellahi, M. Mamourian, and M. Moghiman, Int. J. Heat Mass Transf. **107**, 1110 (2017).

[45] M. A. Sheremet, D. C. Cimpean, and I. Pop, Appl. Therm. Eng. **113**, 413 (2017).
[46] C. C. Cho, Int. J. Heat Mass Transf. **101**, 637 (2016).
[47] S. Siddiqa, M. Sulaiman, M. A. Hossain, S. Islam, and R. S. R. Gorla, Int. J. Therm. Sci. **108**, 244 (2016).
[48] M. A. Sheremet, H. F. Oztop, I. Pop, and K. Al-Salem, Int. J. Heat Mass Transf. **103**, 955 (2016).
[49] P. K. Kameswaran, B. Vasu, P. V. S. N. Murthy, and R. S. R. Gorla, Int. Commun. Heat Mass Transf. **77**, 78 (2016).
[50] M. A. Hossain and I. Pop, Act. Mech. **48**, 813 (1996).
[51] S. E. Ahmed and M. A. El-Aziz, Meccanica **48**, 33 (2013).
[52] R. S. R. Gorla and M. Kumari, J. Nano Engng. Nano Sys. **225**, 133 (2011).
[53] L. S. Yao, ASME J. Heat Transf. **105**, 465 (1983).
[54] S. G. Moulic and L. S. Yao, ASME J. Heat Transf. **111**, 1106 (1989).
[55] M. M. Molla, M. A. Hossain, and L. S. Yao, Int. J. Therm. Sci. **43**, 157 (2004).
[56] K. H. Kabir, M. A. Alim, and L. S. Andallah, A. J. Comp. Math. **3**, 91 (2013).
[57] C. Y. Cheng, Int. Comm. Heat Mass Transf. **26**, 935 (1999).
[58] A. Mehmood, M. S. Iqbal, and I. Mustafa, Zeitschrift für Naturforschung A **71**, 583 (2016).
[59] A. Mehmood and M. S. Iqbal, Therm. Sci. **22**, (2016), DOI: TSCI1151008122M.
[60] A. Mehmood and M. S. Iqbal, J. Mol. Liq. **223**, 1178 (2016).
[61] A. Mehmood and M. S. Iqbal, J. Mol. Liq. **224**, 1326 (2016).
[62] T. Cebeci and P. Bradshaw, Springer New York, 1988.
[63] T. Y. Na, Academic Press New York, 1979.
[64] M. A. Alim, S. Alam, and M. Miraj, Int. J. Eng. Tech. **11**, 60 (2011).
[65] M. A. Hossain, S. Kabir, and D. S. A. Rees, ZAMP **53**, 48 (2002).